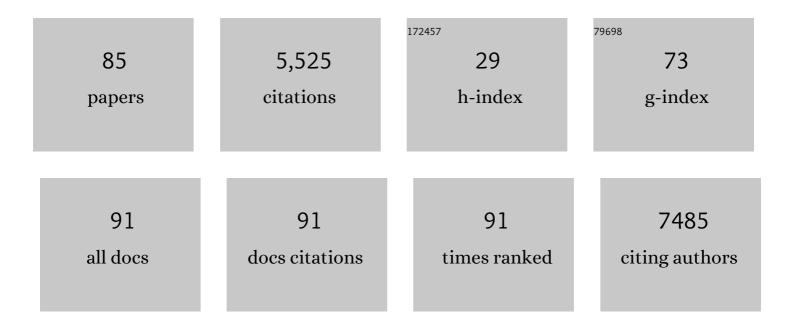
## Jianguo Wen

List of Publications by Year in descending order

Source: https://exaly.com/author-pdf/4193754/publications.pdf Version: 2024-02-01



#	Article	IF	CITATIONS
1	High Nickel and No Cobalt─The Pursuit of Next-Generation Layered Oxide Cathodes. ACS Applied Materials & Interfaces, 2022, 14, 23056-23065.	8.0	30
2	Electrospun porous La–Sr–Co–Ni–O nanofibers for highly sensitive non-enzymatic glucose detection. Materials Advances, 2022, 3, 2096-2103.	5.4	6
3	Rare-earth-doped electrospun scheelite CaWO4 nanofibers with excitation-dependent photoluminescence and high-linearity cathodoluminescence for ratiometric UV wavelength and radiation sensors. Optical Materials, 2022, 126, 112130.	3.6	7
4	Achieving High Stability and Performance in P2â€Type Mnâ€Based Layered Oxides with Tetravalent Cations for Sodiumâ€Ion Batteries. Small, 2022, 18, e2201086.	10.0	25
5	Machine learning the metastable phase diagram of covalently bonded carbon. Nature Communications, 2022, 13, .	12.8	9
6	Origin of structural degradation in Li-rich layered oxide cathode. Nature, 2022, 606, 305-312.	27.8	206
7	Size- and concentration-dependent Eu2+/Eu3+ mixed luminescent characteristics of rare-earth-doped CaF2 nanoparticles and their monolithic epoxy nanocomposites. Journal of Alloys and Compounds, 2021, 857, 157591.	5.5	18
8	Ultrathin Porous Hydrocarbon Membranes Templated by Nanoparticle Assemblies. Nano Letters, 2021, 21, 166-174.	9.1	6
9	Effects of Superparamagnetic Iron Nanoparticles on Electrocatalysts for the Reduction of Oxygen. Inorganic Chemistry, 2021, 60, 4236-4242.	4.0	2
10	Dopant site-dependent luminescence from rare-earth doped dibarium octafluorohafnate Ba <sub>2</sub> HfF <sub>8</sub> nanocubes for radiation detection. Journal of Materials Chemistry C, 2021, 9, 1721-1729.	5.5	8
11	Amorphization mechanism of SrIrO <sub>3</sub> electrocatalyst: How oxygen redox initiates ionic diffusion and structural reorganization. Science Advances, 2021, 7, .	10.3	122
12	Discovery of Gold Nanoparticles in Marcellus Shale. ACS Earth and Space Chemistry, 2021, 5, 129-135.	2.7	4
13	Bifunctional Janus Particles as Multivalent Synthetic Nanoparticle Antibodies (SNAbs) for Selective Depletion of Target Cells. Nano Letters, 2021, 21, 875-886.	9.1	24
14	High-Rate Long Cycle-Life Li-Air Battery Aided by Bifunctional InX <sub>3</sub> (X = I and Br) Redox Mediators. ACS Applied Materials & Interfaces, 2021, 13, 4915-4922.	8.0	17
15	Insights into the extraction of photogenerated holes from CdSe/CdS nanorods for oxidative organic catalysis. Journal of Materials Chemistry A, 2021, 9, 12690-12699.	10.3	8
16	Understanding Co roles towards developing Co-free Ni-rich cathodes for rechargeable batteries. Nature Energy, 2021, 6, 277-286.	39.5	255
17	Advanced nanoscale characterization of aluminum nanoparticles with modified surface morphology via atmospheric helium and carbon monoxide plasmas. Journal of Applied Physics, 2021, 129, .	2.5	7
18	Two-dimensional superconductivity and anisotropic transport at KTaO <sub>3</sub> (111) interfaces. Science, 2021, 371, 716-721.	12.6	136

#	Article	IF	CITATIONS
19	Alloying–realloying enabled high durability for Pt–Pd-3d-transition metal nanoparticle fuel cell catalysts. Nature Communications, 2021, 12, 859.	12.8	137
20	Intermediate Sr <sub>2</sub> Co <sub>1.5</sub> Fe <sub>0.5</sub> O <sub>6â~îî</sub> Tetragonal Structure between Perovskite and Brownmillerite as a Model Catalyst with Layered Oxygen Deficiency for Enhanced Electrochemical Water Oxidation. ACS Catalysis, 2021, 11, 4327-4337.	11.2	31
21	Molecular beam epitaxy of PdO on MgO (001). Physical Review Materials, 2021, 5, .	2.4	1
22	Process Engineering to Increase the Layered Phase Concentration in the Immediate Products of Flame Spray Pyrolysis. ACS Applied Materials & amp; Interfaces, 2021, 13, 26915-26923.	8.0	11
23	Stabilized Lithium, Manganese-Rich Layered Cathode Materials Enabled by Integrating Co-Doping and Nanocoating. ACS Applied Materials & Interfaces, 2021, 13, 22597-22607.	8.0	21
24	Cathodoluminescence of alkaline earth hexafluorometallate nanowires. Microscopy and Microanalysis, 2021, 27, 3276-3278.	0.4	0
25	Photo-induced ultrafast phase transition in twisted bilayer graphene. Microscopy and Microanalysis, 2021, 27, 2954-2956.	0.4	0
26	Unveiling the roles of Co and Mn in structural stability for Ni-rich Cathodes. Microscopy and Microanalysis, 2021, 27, 3436-3438.	0.4	2
27	New Compounds and Phase Selection of Nickel Sulfides via Oxidation State Control in Molten Hydroxides. Journal of the American Chemical Society, 2021, 143, 13646-13654.	13.7	10
28	Superconductivity in Y <sub>4</sub> RuGe <sub>8</sub> with a Vacancy-Ordered CeNiSi <sub>2</sub> -Type Superstructure. Chemistry of Materials, 2021, 33, 7839-7847.	6.7	3
29	Valence Effects of Fe Impurity for Recovered LiNi <sub>0.6</sub> Co <sub>0.2</sub> Mn <sub>0.2</sub> O <sub>2</sub> Cathode Materials. ACS Applied Energy Materials, 2021, 4, 10356-10367.	5.1	11
30	Identifying Support Effects in Au-Catalyzed CO Oxidation. ACS Catalysis, 2021, 11, 11921-11928.	11.2	4
31	Electric field control of magnon spin currents in an antiferromagnetic insulator. Science Advances, 2021, 7, eabg1669.	10.3	12
32	(S)TEM-EELS as an advanced characterization technique for lithium-ion batteries. Materials Chemistry Frontiers, 2021, 5, 5186-5193.	5.9	20
33	Rational design of mechanically robust Ni-rich cathode materials via concentration gradient strategy. Nature Communications, 2021, 12, 6024.	12.8	80
34	Spontaneous formation of anisotropic microrods from paraffin wax in an aqueous environment. Soft Matter, 2021, 18, 156-161.	2.7	1
35	Magnetic Effect of Dopants on Bright and Dark Excitons in Strongly Confined Mn-Doped CsPbl <sub>3</sub> Quantum Dots. Nano Letters, 2021, 21, 9543-9550.	9.1	12
36	ScOx rich surface terminations on lanthanide scandate nanoparticles. Physical Review Materials, 2021, 5, .	2.4	1

#	Article	IF	CITATIONS
37	Catalytically Active Oil-Based Lubricant Additives Enabled by Calcining Ni–Al Layered Double Hydroxides. Journal of Physical Chemistry Letters, 2020, 11, 113-120.	4.6	31
38	Ultrafast formation of a transient two-dimensional diamondlike structure in twisted bilayer graphene. Physical Review B, 2020, 102, .	3.2	8
39	Surfaceâ€Mediated Interconnections of Nanoparticles in Cellulosic Fibrous Materials toward 3D Sensors. Advanced Materials, 2020, 32, e2002171.	21.0	18
40	Tribochemical Conversion of Methane to Graphene and Other Carbon Nanostructures: Implications for Friction and Wear. ACS Applied Nano Materials, 2020, 3, 8060-8067.	5.0	32
41	Enhanced long-term cyclability in Li-Rich layered oxides by electrochemically constructing a LixTM3-xO4-type spinel shell. Nano Energy, 2020, 77, 105188.	16.0	29
42	Predicting Morphological Evolution during Coprecipitation of MnCO <sub>3</sub> Battery Cathode Precursors Using Multiscale Simulations Aided by Targeted Synthesis. Chemistry of Materials, 2020, 32, 9126-9139.	6.7	15
43	Facile and scalable dry surface doping technique to enhance the electrochemical performance of LiNi0.64Mn0.2Co0.16O2 cathode materials. Journal of Materials Chemistry A, 2020, 8, 19866-19872.	10.3	12
44	Activation of Low-Valent, Multiply M–M Bonded Group VI Dimers toward Catalytic Olefin Metathesis via Surface Organometallic Chemistry. Organometallics, 2020, 39, 1035-1045.	2.3	8
45	Two-way tuning of structural order in metallic glasses. Nature Communications, 2020, 11, 314.	12.8	29
46	Visualizing Anisotropic Oxygen Diffusion in Ceria under Activated Conditions. Physical Review Letters, 2020, 124, 056002.	7.8	12
47	Epitaxial Er-doped Y2O3 on silicon for quantum coherent devices. APL Materials, 2020, 8, .	5.1	23
48	Chemisorption-Driven Roughening of Hydrothermally Grown KTa <sub>1–<i>x</i></sub> Nb <sub><i>x</i></sub> O <sub>3</sub> Nanoparticles. Journal of Physical Chemistry C, 2020, 124, 7988-7993.	3.1	3
49	Structure of the (110) <mml:math xmlns:mml="http://www.w3.org/1998/Math/MathML"&gt; <mml:mrow> <mml:mi>L</mml:mi> <mml:mi>nmathvariant="normal"&gt;O</mml:mi> <mml:mn>3</mml:mn> <mml:mo>Â</mml:mo> <mml:mo> (surfaces. Physical Review Materials. 2020. 4.</mml:mo></mml:mrow></mml:math 	> <mml:mi: nml:mo&gt;&lt;</mml:mi: 	>Sc៹/mml:mi mml:mi>L
50	Complex Fluorine Chemical Potential Effects on the Shape and Compositional Heterogeneity of KTa <sub>1–<i>x</i></sub> Nb <i><sub>x</sub></i> O <sub>3</sub> Nanoparticles. Journal of Physical Chemistry C, 2020, 124, 26012-26017.	3.1	1
51	Semi-artificial Photosynthetic CO <sub>2</sub> Reduction through Purple Membrane Re-engineering with Semiconductor. Journal of the American Chemical Society, 2019, 141, 11811-11815.	13.7	44
52	Selective Growth of a Discontinuous Subnanometer Pd Film on Carbon Defects for Li–O <sub>2</sub> Batteries. ACS Energy Letters, 2019, 4, 2782-2786.	17.4	50
53	Correlation between manganese dissolution and dynamic phase stability in spinel-based lithium-ion battery. Nature Communications, 2019, 10, 4721.	12.8	182
54	<i>In Situ</i> Formed Ir <sub>3</sub> Li Nanoparticles as Active Cathode Material in Li–Oxygen Batteries. Journal of Physical Chemistry A, 2019, 123, 10047-10056.	2.5	11

#	Article	IF	CITATIONS
55	Enhanced Electrochemical Performance of Sodium Manganese Ferrocyanide by Na <sub>3</sub> (VOPO <sub>4</sub> ) <sub>2</sub> F Coating for Sodium-Ion Batteries. ACS Applied Materials & Interfaces, 2019, 11, 37685-37692.	8.0	33
56	Pressure-induced tuning of lattice distortion in a high-entropy oxide. Communications Chemistry, 2019, 2, .	4.5	53
5 <b>7</b>	Grain Growth in Nanosized Nickel Deformed in a Confining Environment. Journal of Physical Chemistry C, 2019, 123, 13944-13950.	3.1	1
58	Atomistic manipulation of reversible oxidation and reduction in Ag with an electron beam. Nanoscale, 2019, 11, 10756-10762.	5.6	14
59	Electrophilic Organoiridium(III) Pincer Complexes on Sulfated Zirconia for Hydrocarbon Activation and Functionalization. Journal of the American Chemical Society, 2019, 141, 6325-6337.	13.7	38
60	A novel reversible fluorescent probe for the highly sensitive detection of nitro and peroxide organic explosives using electrospun BaWO <sub>4</sub> nanofibers. Journal of Materials Chemistry C, 2019, 7, 14949-14961.	5.5	27
61	Highly crystalline sodium manganese ferrocyanide microcubes for advanced sodium ion battery cathodes. Journal of Materials Chemistry A, 2019, 7, 22248-22256.	10.3	51
62	A stable rhodium single-site catalyst encapsulated within dendritic mesoporous nanochannels. Nanoscale, 2018, 10, 1047-1055.	5.6	17
63	Luminescence characteristics of rare-earth-doped barium hexafluorogermanate BaGeF6 nanowires: fast subnanosecond decay time and high sensitivity in H2O2 detection. RSC Advances, 2018, 8, 39296-39306.	3.6	13
64	Ultralow-loading platinum-cobalt fuel cell catalysts derived from imidazolate frameworks. Science, 2018, 362, 1276-1281.	12.6	735
65	Atomically Precise Strategy to a PtZn Alloy Nanocluster Catalyst for the Deep Dehydrogenation of <i>n</i> -Butane to 1,3-Butadiene. ACS Catalysis, 2018, 8, 10058-10063.	11.2	67
66	Effect of doping on the performance of high-crystalline SrMnO3 perovskite nanofibers as a supercapacitor electrode. Ceramics International, 2018, 44, 21982-21992.	4.8	102
67	Kinetic Growth Regimes of Hydrothermally Synthesized Potassium Tantalate Nanoparticles. Nano Letters, 2018, 18, 5186-5191.	9.1	14
68	Fast luminescence from rare-earth-codoped BaSiF6 nanowires with high aspect ratios. Journal of Materials Chemistry C, 2018, 6, 7285-7294.	5.5	17
69	Tribological Behavior of NiAl-Layered Double Hydroxide Nanoplatelets as Oil-Based Lubricant Additives. ACS Applied Materials & Interfaces, 2017, 9, 30891-30899.	8.0	59
70	Synthesis of quenchable amorphous diamond. Nature Communications, 2017, 8, 322.	12.8	74
71	Dynamics of Transformation from Platinum Icosahedral Nanoparticles to Larger FCC Crystal at Millisecond Time Resolution. Scientific Reports, 2017, 7, 17243.	3.3	9
72	Enabling the high capacity of lithium-rich anti-fluorite lithium iron oxide by simultaneous anionic and cationic redox. Nature Energy, 2017, 2, 963-971.	39.5	140

#	Article	IF	CITATIONS
73	Rate mechanism of vanadium oxide coated tin dioxide nanowire electrode for lithium ion battery. Nano Energy, 2017, 42, 294-299.	16.0	18
74	A lithium–oxygen battery based on lithium superoxide. Nature, 2016, 529, 377-382.	27.8	633
75	The Effect of Potassium Impurities Deliberately Introduced into Activated Carbon Cathodes on the Performance of Lithium–Oxygen Batteries. ChemSusChem, 2015, 8, 4235-4241.	6.8	13
76	Interfacial Effects on Lithium Superoxide Disproportionation in Li-O <sub>2</sub> Batteries. Nano Letters, 2015, 15, 1041-1046.	9.1	92
77	Growth of Au on Pt Icosahedral Nanoparticles Revealed by Low-Dose In Situ TEM. Nano Letters, 2015, 15, 2711-2715.	9.1	106
78	Effectively suppressing dissolution of manganese from spinel lithium manganate via a nanoscale surface-doping approach. Nature Communications, 2014, 5, 5693.	12.8	255
79	Imaging the Atomic Surface Structures of CeO <sub>2</sub> Nanoparticles. Nano Letters, 2014, 14, 191-196.	9.1	183
80	Effect of the size-selective silver clusters on lithium peroxide morphology in lithium–oxygen batteries. Nature Communications, 2014, 5, 4895.	12.8	186
81	A nanostructured cathode architecture for low charge overpotential in lithium-oxygen batteries. Nature Communications, 2013, 4, 2383.	12.8	379
82	Doubling the critical current density of high temperature superconducting coated conductors through proton irradiation. Applied Physics Letters, 2013, 103, .	3.3	70
83	Observation of Microstructural Evolution in Li Battery Cathode Oxide Particles by In Situ Electron Microscopy. Advanced Energy Materials, 2013, 3, 1098-1103.	19.5	336
84	Assembly of γ-Fe2O3/polyaniline nanofilms with tuned dipolar interaction. Journal of Nanoparticle Research, 2012, 14, 1.	1.9	21
85	Lithium-Ion Battery Materials as Tunable, "Redox Non-Innocent―Catalyst Supports. ACS Catalysis, 0, , 7233-7242.	11.2	6